ELSEVIER

Materials Science and Engineering A340 (2003) 216–224

MATERIALS SCIENCE & ENGINEERING A

www.elsevier.com/locate/msea

Microstructure evolution during annealing of an amorphous TiAl sheet

O.N. Senkov *, M.D. Uchic

Air Force Research Laboratory, Materials and Manufacturing Directorate, AFRL/MLLMD, Wright-Patterson AFB, OH 45433-7817, USA

Received 28 November 2001; received in revised form 13 March 2002

Abstract

An amorphous, 150 μm thick freestanding sheet of a TiAl-based alloy was produced by physical vapor deposition (PVD). The following phase transformations were observed after different stages of crystallization of the amorphous sheet and analyzed using differential thermal analysis, X-ray diffraction, and transmission electron microscopy: amorphous → body centered cubic (β) → hexagonal close-packed (α)? → tetragonal (γ) + ordered α_2. The β phase was formed as near-spherical particles that were evenly distributed in the amorphous phase and the size of these particles was approximately 90 nm. Formation of the α phase by decomposition of β and the remaining amorphous phases led to a very fine feathery-like microstructure arranged in colonies of approximately 100 nm in size. Interface boundaries between the α phase particles were poorly defined. The transformation of the metastable α phase into a mixture of the γ and α_2 phases led to formation of an equiaxed γ-grain structure with the grain size of approximately 150 nm.

Keywords: Physical vapor deposition; Differential thermal analysis; X-ray diffraction; Amorphous materials; Titanium aluminide; Phase transformations

1. Introduction

Titanium aluminides are currently considered as promising materials for airspace applications because of their low density, reasonable oxidation resistance and high strength at temperatures up to 800 °C [1]. Recently, a significant interest has developed to use these materials in sheet or thin film forms for applications that additionally require low thermal conductivity such as thermal protection systems and structural coatings. However, these materials generally have limited ductility at temperatures below 700 °C. The brittle-to-ductile transition temperature can be decreased and ductility of TiAl alloys can be significantly improved by grain refinement to submicron-size levels [2–4]. Non-equilibrium processes such as rapid solidification, mechanical alloying, and PVD can be effectively used to produce fine-grain structures. Moreover, it has recently been established that TiAl-based alloys can become amorphous when produced by these non-equilibrium techniques [5–11]. The amorphous phase can then be used as a precursor to form a nanocrystalline structure by simultaneous compaction and crystallization through careful control of the time and temperature conditions [7]. Crystallization of the amorphous phase may also lead to formation of metastable phases with novel properties [8–11]. Of course, knowledge of the crystallization kinetics of the amorphous phase and microstructural evolution of crystallized phases is required to properly control the final microstructure and properties.

In the present work, the evolution of the microstructure and phase transformations after different stages of crystallization of a TiAl amorphous sheet were studied using differential thermal analysis (DTA), X-ray diffraction (XRD) and transmission electron microscopy (TEM). Similarities in the phase progression during crystallization from melt and from amorphous state were found. Formation of metastable body centered

* Corresponding author. Address: UES, Inc., 4401 Dayton-Xenia Road, Dayton, OH 45432-1894, USA. Tel.: +1-937-255-1320; fax: +1-937-656-7292

E-mail address: oleg.senkov@wpafb.af.mil (O.N. Senkov).

0921-5093/02/$ - see front matter
PII: S0921-5093(02)00189-2

cubic (BCC) and hexagonal phases was observed and discussed.

2. Experimental procedures

A 150 μm thick freestanding film of a γ-TiAl alloy was deposited using a magnetron sputtering system. A Ti–46.5Al–3Nb–2Cr–0.2Mo (at.%) alloy of potential engineering importance [12] was used as the target material. The experimental procedures used to produce the amorphous film are described in more detail in a previous paper [11].

Crystallization kinetics of the amorphous phase were studied using a Universal V2.3C TA DTA unit. The samples were heated from 50 to 1000 °C in an argon atmosphere. Heating rates of 5, 10, 20, 30 and 50 °C min^{-1} were used to determine the activation enthalpy of the processes controlling crystallization and phase transformations using Kissinger's method [13]. Microstructural characterization was performed on films heated in the DTA unit to selected temperatures at a heating rate of 5 °C min^{-1}, which were then immediately cooled at a rate exceeding 20 °C min^{-1}. XRD was conducted with a Rigaku Rotaflex X-ray diffractometer using Cu Kα radiation. A Phillips CM200 transmission electron microscope operating at 200 kV was used for microstructural investigations. TEM thin foils were prepared in a twin jet electropolisher using an electrolytic solution consisting of 300 ml methanol, 175 ml 2-butanol and 30 ml perchloric acid (70%). During electropolishing, the electrolyte was cooled to −40 °C and a 20 V potential was applied.

3. Results

3.1. Characterization of as-deposited TiAl sheet

An XRD pattern of as-deposited sheet is shown in Fig. 1. A spread halo is present in the 2Θ range of 35–45°, indicating that the sheet is amorphous. TEM bright- and dark-field images, Fig. 2(a) and (b), show even featureless contrast of the as-deposited film and the corresponding selected area diffraction pattern (SADP's), Fig. 2(d) exhibits a halo; these characteristics are typical of an amorphous state. However, a small volume fraction (< 1 vol.%) of a crystalline phase was also detected by TEM, which is illustrated in Fig. 2. The size of these crystalline inclusions was less than 500 nm and they consisted of very fine, approximately 20 nm diameter, grains, Fig. 2(c). This crystalline phase was identified as a disordered hexagonal close-packed (HCP) α phase. Fig. 2(e) shows a SADP taken from a crystalline inclusion with the incident beam parallel to the $[0\ 0\ 0\ 1]_\alpha$ zone of one of the grains. The diffraction spots were identified to belong to the α phase with the lattice parameters $a = 0.292$ nm and $c = 0.47$ nm.

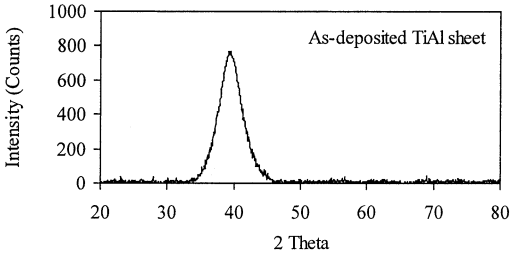

Fig. 1. XRD pattern of a TiAl foil produced by PVD in the as-deposited condition.

DTA of the amorphous as-deposited material shows three exothermic reactions in the temperature range of 50 to 1000 °C during heating at a rate of 5 °C min^{-1}, with reaction maxima at 523, 537, and 648 °C, Fig. 3.

Fig. 4 shows the effect of heating rate on kinetics of crystallization and phase transformations in the PVD TiAl-based sheet. All reactions shift towards higher temperatures when the heating rate increases. However, the magnitudes of the peak shifts are different for the three reactions. Further, the first and second peaks become superimposed at heating rates of 20 °C min^{-1} and higher. According to Kissinger [12], the activation energy, E, of the process controlling the transformation is given by the following equation:

$$E = -R\mathrm{d}[\ln(v/T_\mathrm{p}^2)]/\mathrm{d}(1/T_\mathrm{p}) \quad (1)$$

where v is the heating rate, T_p is the peak maximum temperature, and R is the gas constant. Therefore, the activation energy can be determined from slopes of the curves $\ln(v/T_\mathrm{p}^2)$ versus $1/T_\mathrm{p}$. These curves are plotted in Fig. 5 for each of the three exothermic reactions, and all three reactions display a linear dependency. The activation energies for the first, second and third exothermic peaks are evaluated to be 315 ± 10, 365 ± 50, and 325 ± 10 kJ mol^{-1}, respectively.

3.2. Characterization of crystallization transformations in heat treated sheet

To understand the origin of the exothermic reactions occurring during continuous heating of the amorphous sheet, samples were heated in the DTA at a rate of 5 °C min^{-1} to 520, 530, 600 and 850 °C (the corresponding locations on the DTA curve are shown in Fig. 3). After reaching the desired temperature, the samples were immediately cooled and analyzed with the use of XRD and TEM.

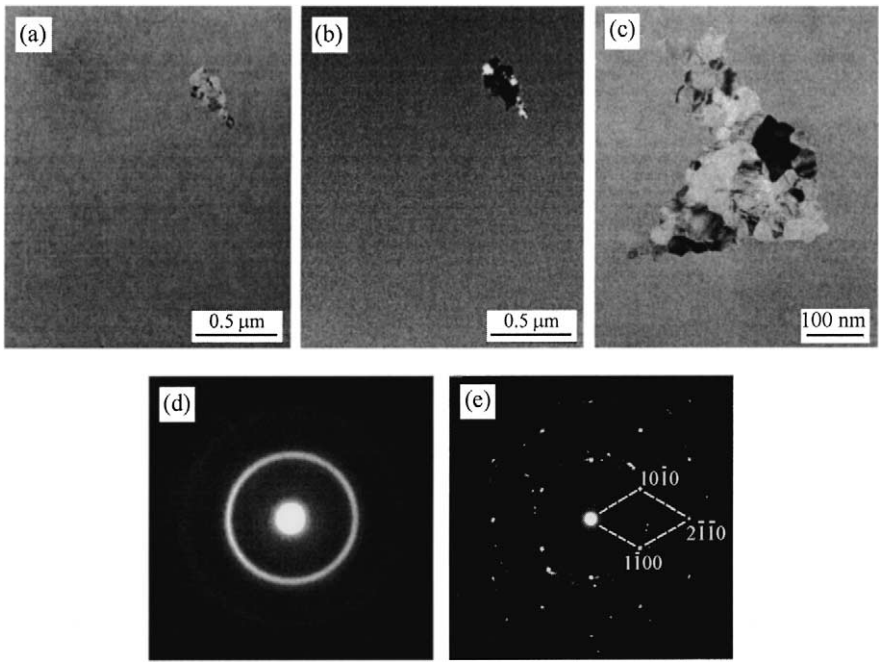

Fig. 2. (a) Bright-field and (b) dark-field TEM images of the as-deposited amorphous TiAl sheet, (c) bright-field image of a crystalline inclusion, and (d, e) corresponding SADP's from (d) the amorphous and (e) crystalline regions. The reciprocal lattice cell of the [0 0 0 1] zone from the disordered α-Ti phase with the h.c.p. crystal structure is also shown in (e).

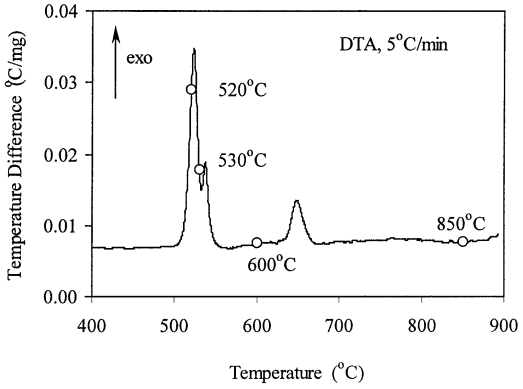

Fig. 3. DTA curve of an amorphous TiAl sheet produced by PVD. Heating rate is 5 °C min^{-1}. Characteristic points of the DTA curve to which several specimens were heated for the following XRD and TEM analyses are indicated by open circles and the corresponding temperatures are given.

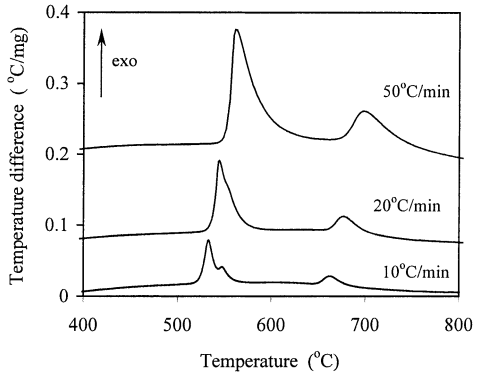

Fig. 4. DTA curves of the amorphous TiAl sheet produced by PVD. The DTA curves were obtained during heating with the heating rates of 10, 20 and 50 °C min^{-1}.

3.3. Phases and microstructures associated with the first exothermic reaction

Three intense XRD peaks from a crystalline phase together with a halo from a residual amorphous phase are detected after heating to 520 °C (i.e. 3 °C below the maximum for the first exothermic reaction), as shown in Fig. 6(a). The crystalline phase was identified as the BCC β phase with the lattice parameter $a = 0.3195$ nm. Near-spherical crystalline particles of approximately 90 nm in size were detected in the amorphous matrix by TEM after this annealing condition, as seen in Fig. 7(a) and (b). A selective area diffraction pattern (SADP's) shown in Fig. 7(c) contains a halo from the amorphous phase and rings from the crystalline β phase, in agreement with the corresponding XRD data. Energy dispersive spectroscopy showed that the crystalline particles had the following compositions (in at.%): 52–57 Ti, 37–42 Al, 2.0–2.2 Cr, 2.5–3.0 Nb, 0.6–1.0 Mo, which is close to the average composition of the target material.

A slight increase in the annealing temperature to 530 °C led to a considerable change in the microstructure, as shown in Fig. 8. The most noticeable feature was the complete crystallization of the amorphous phase. In addition, the near-spherical particles were slightly larger (~100 nm in size) and a specific moiré contrast appeared inside the particles, which can be observed in Fig. 8(d). The latter was probably due to precipitation of

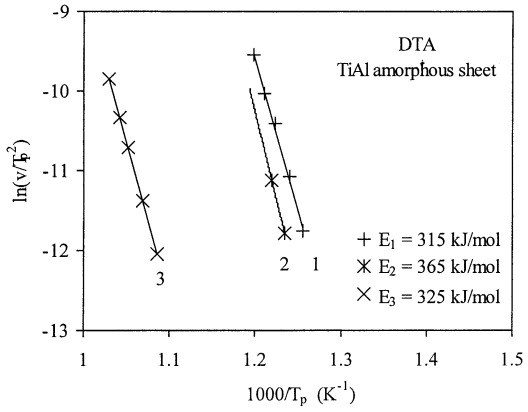

Fig. 5. Dependencies of the logarithm of the heating rate (in K min^{-1}) normalized to the square of the peak temperature T_p on the reciprocal peak temperature for the first, second and third exothermic peaks. The activation energies calculated from the corresponding slopes are given in the plot area.

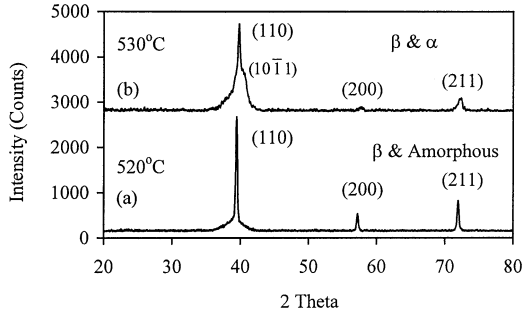

Fig. 6. XRD patterns of the TiAl sheet after annealing at (a) 520 and (b) 530 °C.

an additional crystalline phase, leading to a finer microstructure, Fig. 8(a) and (b). The SADP shown in Fig. 8(c) supports the presence of an additional crystalline phase, as it contains diffraction rings and spots, which do not belong to the β phase. This additional phase was identified as a hexagonal phase with the lattice parameters $a = 0.29$ nm and $c = 0.47$ nm. XRD analysis showed that, in spite of the considerable changes in microstructure observed in the TEM, the β phase is still the major phase at this temperature, see Fig. 6(b). The diffraction lines from this phase are however wider indicating the particle fragmentation and an increase in the intensity of internal stresses, and the most intense (1 0 $\bar{1}$ 1) peak from the α phase can also be identified.

3.4. Phases and microstructures associated with the second and third exothermic reactions

Heating the specimen to 600 °C, i.e. above the second exothermic reaction but below the third one (Fig. 3), resulted in the XRD pattern shown in Fig. 9(a). No β phase was detected and the wide XRD peaks were identified as belonging to a disordered HCP α phase, with the lattice parameters $a = 0.289$ nm and $c = 0.460$ nm. The intensities of the XRD peaks from this phase were much smaller and the peaks were wider as compared to the XRD peaks from the BCC β phase, which may indicate that the grains of the α phase were much finer than the grains of the β phase. TEM analysis confirmed this observation, see Fig. 10. Although the microstructural elements were hardly identified in a bright-field condition, Fig. 10(a), they were clearly seen in a dark-field condition, Fig. 10(b). The main feature of this microstructure is polygonal-shaped grains of approximately 100 nm in size, instead of near-spherical particles in the samples annealed at lower temperatures. The grains were fragmented into finer lamellae, which had irregular orientations producing feathery-like contrasts in bright-field images. Phase analysis also confirmed that there was no β phase present in this sample; instead, the α phase was identified as the only phase, see Fig. 10(c).

After heating to 850 °C, i.e. above the third exothermic reaction shown in Fig. 3, two phases were easily identified on the corresponding XRD pattern, Fig. 9(b). These are the ordered HCP α_2 phase and the tetragonal γ phase. The diffraction peaks from the latter phase were much more intense than those from the α_2 phase, indicating that the γ phase was the major phase in this annealed specimen. The lattice parameters of the γ phase were determined to be $a = 0.4008$ nm and $c = 0.4055$ nm, and the lattice parameters of the α_2 phase were $a = 0.578$ nm and $c = 0.460$ nm. A very well-developed equiaxed γ grain structure, with a grain size of approximately 150 nm, was characteristic of this specimen, Fig. 11. Grain boundaries were clearly visible both in bright and dark-field images, and no precipitates were seen inside the grains on TEM photomicrographs. Some grains were twinned, see Fig. 11(d). SADP's showed diffraction spots from individual grains; these spots were arranged in a number of diffraction rings, Fig. 11(c), and two phases, the major γ and the minor α_2 were identified, in accord to XRD data.

4. Discussion

The results of the present work show that a range of microstructures can be produced during crystallization of the amorphous phase in TiAl sheet made by PVD. The origin of a small amount (< 1 vol.%) of a crystalline clusters that are evenly distributed in the as-deposited sheet can be twofold. One possibility is a selective crystallization of the amorphous phase during sputtering. Another possibility is the non-homogeneous erosion of the target surface (i.e. formation of extended cones on the target surface [14–16]), that may lead to sputtering relatively large (up to 500 nm) pieces from time to time.

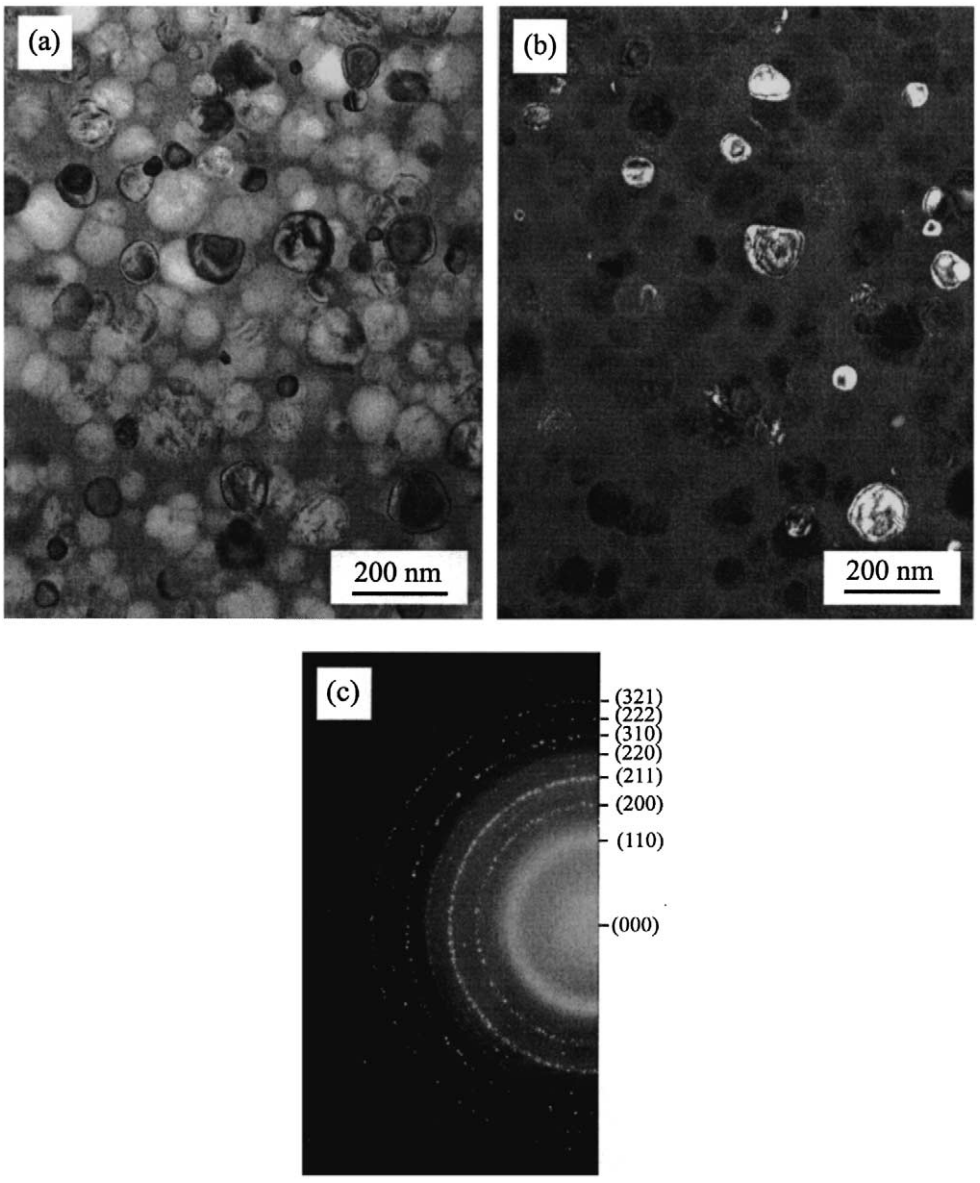

Fig. 7. (a) Bright-field, (b) dark-field TEM images and (c) corresponding indexing SADP of the sheet sample heated to 520 °C.

The first possibility can easily be rejected because relatively high (> 500 °C) temperatures are required to form crystalline particles from the amorphous state. Furthermore, the crystalline particles formed from the amorphous phase are generally round-shaped while the inclusions in the as-deposited sheet have irregular shape (compare Fig. 2 with Figs. 7 and 8). Therefore, the second reason is the most likely, especially if the high deposition rate is taken into account. However, it is evident that these α phase inclusions were not deposited as solid pieces of the target material, but rather they were initially melted and then rapidly solidified on the substrate. This conclusion is based on the observation of a very fine-grain structure (grain size is ≈20 nm) within the crystalline inclusions, which is not typical of the target material that was predominantly γ-phase. In the alloy of the given composition, the α phase is thermodynamically stable only at high temperatures (> 1100 °C), and it is known that the $\alpha \rightarrow \alpha_2$ ordering can only be suppressed by rapid solidification [7,17]. Crystalline particles embedded in the TiAl amorphous phase were also observed by Banerjee et al. [10] and these particles were also identified as a disordered hexagonal α phase of the composition close to the nominal composition of the alloy. However, the crystalline particles in [10] had near-spherical morphology, similar to that shown in Fig. 8, indicating that they were probably formed by crystallization from the amorphous state.

The amorphous phase produced by PVD is rather stable, in spite of presence of the crystalline inclusions, and crystallization starts only after heating to approximately 500 °C. For example, at a heating rate of

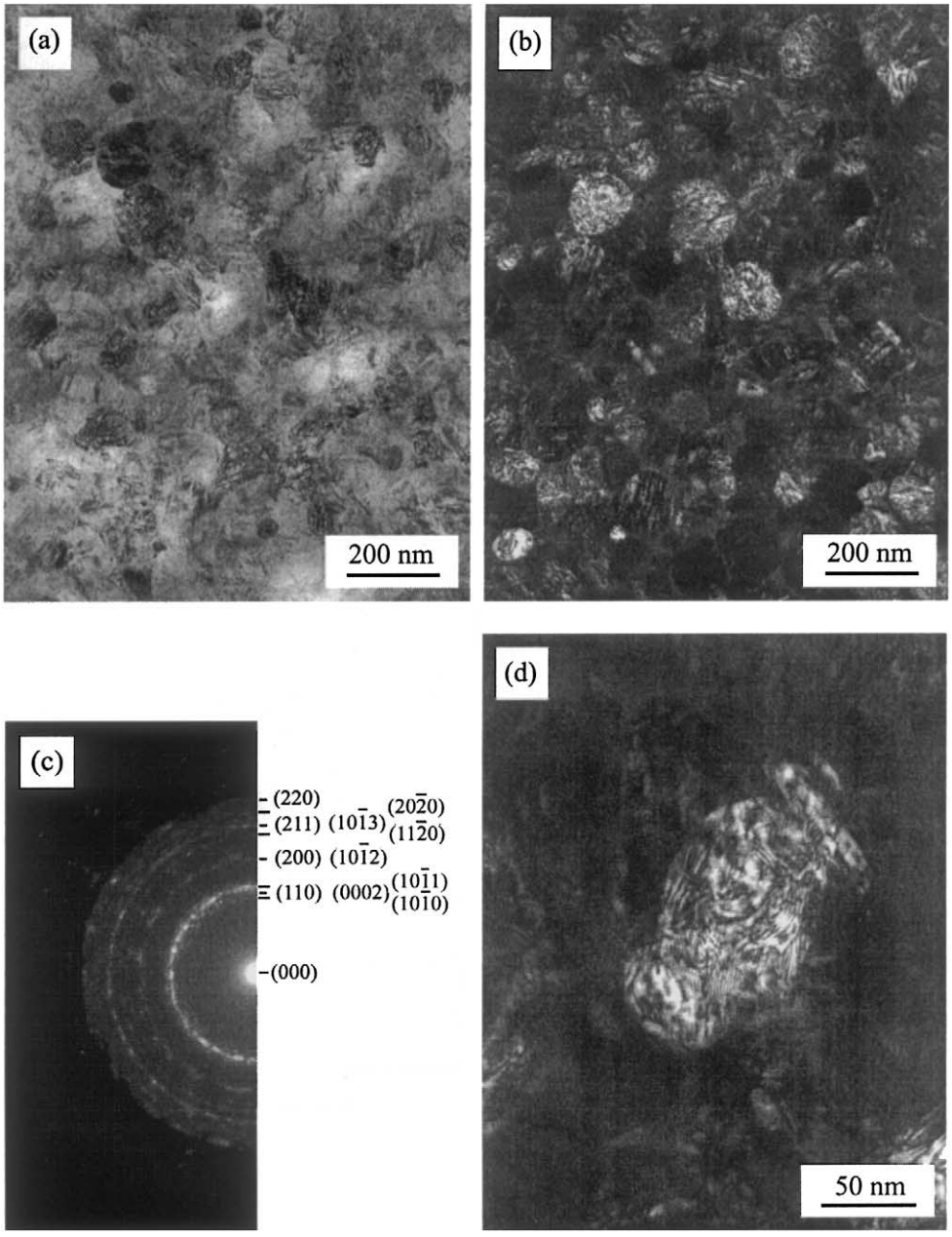

Fig. 8. (a) Bright-field, (b) dark-field images and (c) corresponding indexing SADP of the sheet sample heated to 530 °C, the presence of two phases, BCC and HCP, is evident, (d) dark-field image of an individual fragmented particle.

5 °C min^{-1}, crystallization of the amorphous phase initiates at 513 °C with the formation of near-spherical particles of the metastable BCC β phase. The size of the β-phase particles is approximately 90 nm and they are homogeneously distributed in the amorphous phase. These particles have near the same chemistry as the amorphous phase, which is typical of a nucleation from a highly undercooled liquid.

The metastable β phase is present only in a very narrow temperature range, and it transforms into the HCP α phase at a temperature range of 530–545 °C. Irregularly shaped (mostly elongated) very fine particles of the α phase precipitate inside the β particles and the remaining amorphous phase, producing a feathery-like microstructure with not very well defined interface boundaries. This phase is also metastable, and it transforms into the tetragonal γ and ordered hexagonal α_2 phases at temperatures above ~640 °C. Because of different transformation kinetics, the temperature range between starting formation of the β and α phases decreases when the heating rate is increased, and these transformations become superimposed at heating rates of 20 °C min^{-1} and higher. As a result, the amorphous phase crystallizes directly to the α phase, without

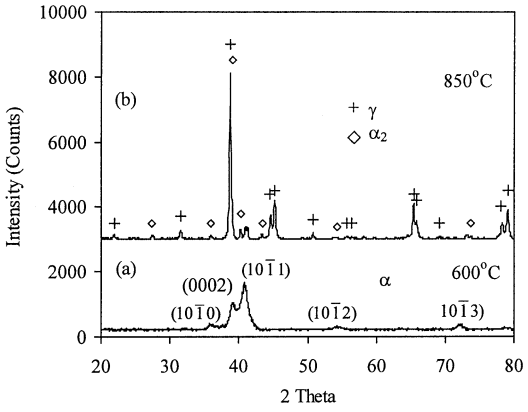

Fig. 9. XRD patterns of the TiAl sheet after annealing at (a) 600 and (b) 850 °C.

intermediate formation of the β phase when the heating rate exceeds 20 °C min^{-1}. The activation energies were determined for the first, second and third exothermic peaks to be 315 kJ mol^{-1} (for amorphous-to-β), 365 kJ mol^{-1} (for β-to-α), and 325 kJ mol^{-1} (for α to α_2 and γ), respectively. These values can be compared with the activation energies for self-diffusion in β-Ti (250 kJ mol^{-1}) [18] and α-Ti (193 kJ mol^{-1}) [19], volume interdiffusion in α_2 (312 kJ mol^{-1}) and γ (295 kJ mol^{-1}) phases [20], and volume diffusion of Ti in the γ phase (291 kJ mol^{-1}) [21].

The values of self-diffusion in α-Ti and β-Ti are too low to provide agreement with the measured activation energies. Further, diffusion in elemental Ti is not likely to represent a relevant physical process in the current

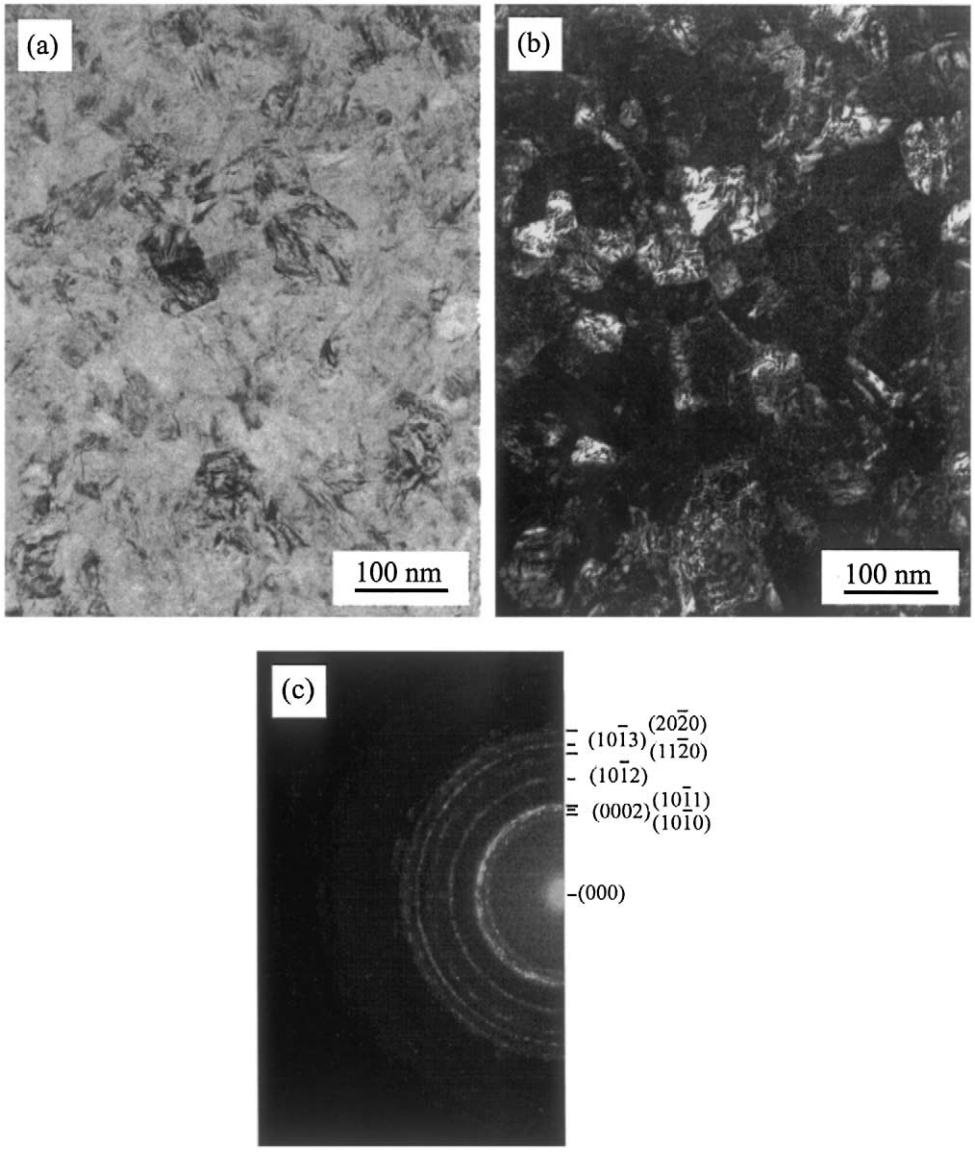

Fig. 10. (a) Bright-field, (b) dark-field TEM images and (c) corresponding SADP of the sheet sample heated to 600 °C.

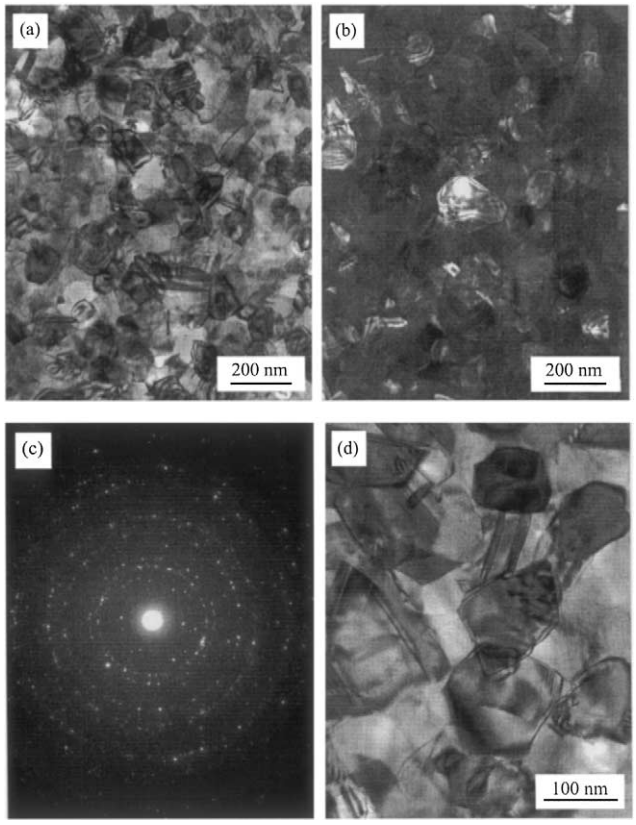

Fig. 11. (a) Bright-field, (b) dark-field TEM images and (c) corresponding SADP of the sheet sample heated to 850 °C. (d) TEM photomicrograph showing twinned γ grains.

alloy with a high Al concentration. As the first two transformations established here represent reactions that are far from equilibrium, they may be difficult to relate to physical processes that have been characterized in equilibrium crystalline structures. On the other hand, the measured activation energy of 325 kJ mol^{-1} for the transformation from α to $\gamma+\alpha_2$ in the present study is within 10% of the values cited for volume diffusion in α_2 (312 kJ mol^{-1}) and γ (295 kJ mol^{-1}), and for Ti diffusion in γ (291 kJ mol^{-1}). Each of these mechanisms are possible rate-limiting reactions for this final transformation. However, the current measurements are unable to distinguish between these three possible mechanisms.

Formation of the BCC β phase during crystallization of the amorphous phase in TiAl has been reported for the first time. In equilibrium conditions, this phase is present only at near melting temperatures [17]. In fact, this is the first crystalline phase formed during crystallization from melt. The lattice parameter of the β phase formed from the amorphous state ($a=0.3195$ nm) is similar to that of the β phase formed from the melt ($a \cong 0.33$ nm), if the thermal expansion is taken into account. Therefore, these BCC phases can be considered to be of the same nature and the β phase formed from the amorphous phase should be considered as a metastable phase.

Metastable primitive cubic phase with the lattice parameter $a=0.69$ nm [9] and a tetragonal phase with the lattice parameters $a=0.688$ nm and $c=0.710$ nm [10] were detected using TEM during crystallization of an amorphous phase in TiAl foils produced by magnetron sputtering. The tetragonal phase was observed only in very thin regions of TEM specimens and only during in situ experiments at temperatures above 600 °C, and its origin was related to contamination of these regions with oxygen or nitrogen [10]. The primitive cubic phase was discovered in thicker foils annealed at 527 °C for 1 h and it was identified to be similar to β-Mn [9]. It is interesting that the transformation of the BCC β phase into the α phase was observed in our work in almost the same temperature range (525–535 °C) where the primitive cubic phase was observed in [9]. However, a thorough TEM analysis did not show any evidence of the presence of an additional phase with large lattice parameters (the metastable primitive cubic or tetragonal phases) in our material after annealing at temperatures below the third exothermic reaction. In this temperature range, the diffraction spots, which were the closest to the central spot in the SADP's, were reflected from the (1 0 $\bar{1}$ 0) α planes, see Figs. 7 and 8.

The transformation from the amorphous structure to α and then from α to γ and α_2 phases were accounted for in an earlier study of amorphous TiAl based alloys prepared by mechanical alloying [7,8]; however, higher temperatures of the transformations were reported than were shown in our work. The difference in the results may be due to contamination of the mechanically alloyed powder with interstitial elements, which may stabilize the amorphous phase. It should also be noted that only one heating rate of 20 °C min^{-1} was used in [7,8], and we have shown that the β phase cannot be detected at this high heating rate (Fig. 4).

When the sequence of the phase formations during continuous heating of the amorphous sheet is compared with that during continuous cooling from melt, a very similar progression can be seen. Indeed, during crystallization from melt, the first crystalline phase formed is the β phase, which transforms into the α phase by a peritectic reaction [17]. During further cooling, the α phase transforms partially into the γ phase and the remaining α transforms then into a mixture of the α_2 and γ phases by the eutectoid reaction. This similarity supports a general point of view [22] that an amorphous phase can be considered as a highly undercooled liquid and the crystallization kinetics of the amorphous phase should follow the crystallization kinetics of the respective melt.

5. Conclusions

(1) An amorphous sheet of a TiAl-based alloy was produced by PVD methods using a pre-alloyed target, and the sheet thickness was approximately 150 μm.

(2) The amorphous phase was stable at temperatures up to ~ 510 °C, and at higher temperatures, crystallization occurred in two stages. At heating rates below 20 °C min^{-1}, a metastable BCC (β) phase was initially formed which was stable only within a very narrow ($\approx$ 10 °C) temperature range, and then transformed into an HCP (α) phase. At higher heating rates, the amorphous phase transformed directly into the α phase.

(3) The beta phase was formed as near-spherical particles evenly distributed in the amorphous phase. The size of these particles was approximately 90 nm. Formation of the alpha phase by decomposition of the beta and remaining amorphous phases led to a very fine feathery-like microstructure arranged in colonies of approximately 100 nm in size and with poorly defined interface boundaries.

(4) The metastable α phase transformed into a mixture of thermodynamically stable ordered α_2 and tetragonal (γ) phases at temperatures above approximately 640 °C by an exothermic reaction. This transformation led to formation of well-developed equiaxed grains with the grain size of approximately 150 nm.

(5) Activation energies of the processes responsible for the transformations, amorphous $\rightarrow \beta$, $\beta \rightarrow \alpha$ and $\alpha \rightarrow (\gamma + \alpha_2)$, were determined to be 315, 365, and 325 kJ mol^{-1}, respectively.

Acknowledgements

The authors want to thank Dr D.M. Dimiduk and Dr D.B. Miracle, AFRL/MLLM, for discussion of the results and valuable comments, and Dr R. Wheeler, Mr A. Smith, and Mr T. Houston, UES Inc., for help in specimen preparation and characterization. The work was conducted under AFRL contract No. F33615-01-C-5214.

References

[1] K.S. Chan, Y.W. Kim, Acta Metallurgica Mater. 43 (1995) 439.
[2] M.A. Morris, M. Leboeuf, Mater. Sci. Eng. A224 (1997) 1–11.
[3] R.M. Imayev, N.K. Gabdullin, G.A. Salishchev, O.N. Senkov, V.M. Imayev, F.H. Froes, Acta Mater. 47 (1999) 1809–1821.
[4] V.M. Imaev, R.M. Imaev, A.V. Kuznetsov, O.N. Senkov, F.H. Froes, Mater. Sci. Technol. 17 (2001) 566–572.
[5] K. Ameyama, O. Okada, K. Hirai, N. Nakabo, Metall. Trans. JIM 36 (1995) 269.
[6] H. Chang, C.J. Altstetter, R.S. Averback, J. Mater. Res. 7 (1992) 2962–2970.
[7] O.N. Senkov, N. Srisukhumbowornchai, M.L. Ovecoglu, F.H. Froes, J. Mater. Res. 13 (1998) 3399–3410.
[8] O.N. Senkov, M.L. Ovecoglu, N. Srisukhumbowornchai, F.H. Froes, NanoStructured Mater. 10 (1998) 935–945.
[9] E. Abe, M. Ohnuma, M. Nakamura, Acta Mater. 47 (1999) 3607–3616.
[10] R. Banerjee, S. Swaminathan, R. Wheeler, H.L. Fraser, Phil. Mag. A 80 (2000) 1715–1727.
[11] O.N. Senkov, M.D. Uchic, S. Menon, D.B. Miracle, Scripta Materialia 46 (2002) 187–192.
[12] Y.-W. Kim, JOM 46 (7) (1994) 30–39.
[13] H.E. Kissinger, Anal. Chem. 29 (1957) 1702–1705.
[14] A.D.G. Stewart, M.W. Thompson, J. Mater. Sci. 4 (1969) 56.
[15] G.K. Wehner, D.J. Hajicek, J. Appl. Phys. 42 (1971) 1145.
[16] D.J. Elliott, P.D. Towsed, Phil. Mag. 23 (249) (1971) 1261.
[17] Y.-W. Kim, D.M. Dimiduk, in: M.V. Nathal, R. Darolia, C.T. Liu, P.L. Martin, D.B. Miracle, R. Wagner, M. Yamaguchi (Eds.), Structural Intermetallics 1997, TMS, Warrendale, PA, 1997, pp. 531–543.
[18] H. Nakajima, M. Koiwa, ISIJ Internat. 31 (1991) 757–766.
[19] C. Herzig, R. Willecke, K. Vieregge, Phil. Mag. A 63 (1991) 949–958.
[20] W. Sprengel, H. Nakajima, H. Oikawa, Mater. Sci. Eng. A A213 (1996) 45–50.
[21] S. Kroll, H. Mehrer, N. Stolwijk, C. Herzig, R. Rozenkranz, G. Frommeyer, Z. Metallkunde 83 (1992) 591–595.
[22] P.R. Okamoto, N.Q. Lam, L.E. Rehn, Physics of Crystal-to-Glass Transformation, Solid State Physics, Academic Press, New York, 1999, pp. 1–135.